CMS Physics Analysis Summary

Contact: cms-pag-conveners-susy@cern.ch 2016/04/05

Search for supersymmetry in events with photons and missing transverse energy

The CMS Collaboration

Abstract

The results of a search for new physics in final states with photons and missing transverse energy are reported. The study is based on a sample of proton-proton collisions collected at a center-of-mass energy $\sqrt{s} = 13$ TeV with the CMS detector in 2015. The integrated luminosity of the sample is 2.32 fb^{-1}. Many models of new physics, including supersymmetry (SUSY) with general gauge mediation (GGM), predict the production of events with photons, jets, and significant missing transverse energy. The data are used to search for GGM signatures in final states with two photons. No excess is observed with respect to the standard model expectation, and the results are used to set limits on gluino pair production in the GGM SUSY framework.

1 Introduction

Final states in pp collisions with high-p_{T} photons and significant missing transverse energy $E_{\mathrm{T}}^{\mathrm{miss}}$ emerge naturally from a variety of new physics scenarios, particularly in models of supersymmetry (SUSY) broken via gauge mediation and including a stable, weakly interacting lightest supersymmetric particle (LSP) [1–6]. The $E_{\mathrm{T}}^{\mathrm{miss}}$ in the event, defined as the magnitude of the negative vector sum of the p_{T} of the visible particles, is a consequence of the undetected energetic LSPs. Models with general gauge mediation (GGM) can have a wide range of features, but typically entail a gravitino LSP and a next-to-lightest supersymmetric particle (NLSP) commonly taken to be a neutralino.

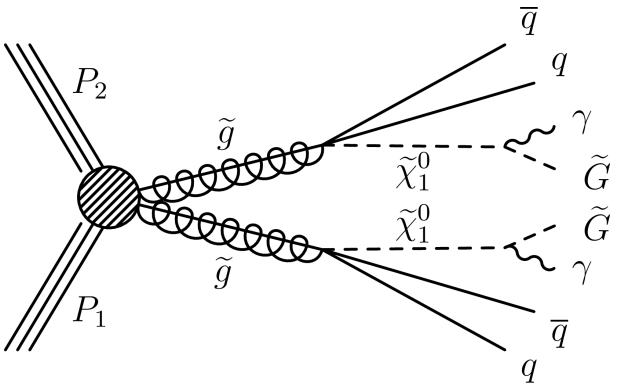

Figure 1: Decay of a gluino $\widetilde{\mathrm{g}}$ to an antiquark, quark, and neutralino, with subsequent decay of the neutralino to a γ and a gravitino $\widetilde{\mathrm{G}}$.

We present here a search for GGM in final states involving two photons. The data sample, corresponding to an integrated luminosity of $2.32\,\mathrm{fb}^{-1}$ of proton-proton collisions at $\sqrt{s} = 13\,\mathrm{TeV}$, was collected with the CMS detector at the LHC in 2015. For the interpretation of the results we assume gluino pair production, with the decay of the gluino shown in Figure 1. In this scenario the NLSP neutralino decays to a gravitino and photon, $\widetilde{\chi}_1^0 \to \widetilde{\mathrm{G}}\gamma$, resulting in characteristic events with jets, two photons, and large $E_{\mathrm{T}}^{\mathrm{miss}}$.

This analysis is based on a search for an excess of events with at least two energetic photons and significant $E_{\mathrm{T}}^{\mathrm{miss}}$ in the final state. We perform a statistical test for the presence of GGM models, and provide additional information relevant to determining the sensitivity of the analysis to other interpretations.

This signature can also arise from several standard model (SM) processes, including direct diphoton production with initial state radiation and multijet events (possibly with associated photon production). These processes lack genuine $E_{\mathrm{T}}^{\mathrm{miss}}$, but can emulate GGM signal topologies if the hadronic activity in the event is poorly measured. In the latter case, photons may be reconstructed in the event as a result of the misidentification of electromagnetically rich jets. A smaller background comes from events with real $E_{\mathrm{T}}^{\mathrm{miss}}$, principally W$\gamma$ and W + jet production, where $\mathrm{W} \to \mathrm{e}\nu_{\mathrm{e}}$ and the electron is misidentified as a photon.

This note is organized as follows: in Section 2 we describe the data samples, simulated signal and background samples, and the trigger criteria used in the analysis. Details of the definitions of particle candidates and the selection of candidate events are described in Section 3. Methods for estimating the primary backgrounds using control samples in data are given in Section 4. Section 5 discusses the systematic uncertainties of the analysis and the results, including exclusion limits, are presented in Section 6. Section 7 summarizes our conclusions.

2 Data and simulated samples

The central feature of the CMS apparatus is a superconducting solenoid of 6 m internal diameter, providing a magnetic field of 3.8 T. Within the superconducting solenoid volume are a silicon pixel and strip tracker covering the pseudorapidity [7] region $|\eta| < 2.5$, as well as a lead tungstate crystal electromagnetic calorimeter (ECAL) and a brass and scintillator hadron calorimeter (HCAL), each composed of a barrel and two endcap sections and covering the range $|\eta| < 3.0$. Forward calorimeters extend the coverage provided by the barrel and endcap detectors. Muons are measured in gas-ionization detectors embedded in the steel flux-return yoke outside the solenoid and cover the range $|\eta| < 2.4$. A more detailed description of the CMS detector, together with a definition of the coordinate system used and the relevant kinematic variables, can be found in Ref. [7].

The data used in this analysis were selected with a diphoton trigger requiring two photons satisfying $p_T > 30$ and 18 GeV, possessing a combined invariant mass $M_{\gamma\gamma} > 95$ GeV, and passing loose photon identification criteria. In addition, the primary standard model backgrounds are studied using events passing diphoton triggers with a lower invariant mass ($M_{\gamma\gamma} > 55$ GeV) but tighter identification requirements on the selected photons. Electron samples used for additional studies were collected by selecting events with a trigger nearly identical to the diphoton trigger, with the additional requirement that both electromagnetic objects be matched to a pixel seed and have an invariant mass $M_{ee} > 70$ GeV.

Monte Carlo (MC) simulations of the signal and background processes are used to validate the performance of the analysis and determine signal efficiencies, as well as to determine the contributions of some of the smaller backgrounds. The leading-order (LO) event generator MADGRAPH 5.1.3.30 [8] was used to simulate the signal samples, which were generated with two gluinos and up to two additional partons. The parton showering, hadronization, multiple-parton interactions, and the underlying event were described by the PYTHIA 6.426 [9] event generator.

The signal events were generated using the T5gg simplified model framework [10] and are characterized by the masses of the particles in the decay chain. The $\widetilde{G}$ mass is taken to be 1 GeV, and a range of masses for the $\widetilde{g}$ was simulated from 1 to 1.8 TeV in 50 GeV increments. For each gluino mass, the $\widetilde{\chi}_1^0$ mass was taken to range from 100 GeV to 1.6 TeV in 100 GeV increments, with the requirement that $M_{\widetilde{\chi}_1^0} < M_{\widetilde{g}}$. We assume branching fractions of unity for the decays $\widetilde{g} \to q\bar{q}\widetilde{\chi}_1^0$ and $\widetilde{\chi}_1^0 \to \widetilde{G}\gamma$.

The production cross sections for these processes are calculated as a function of $M_{\widetilde{g}}$ at NLO accuracy including the resummation of soft gluon emission at next-to-leading logarithmic (NLL) accuracy [11, 12] and the uncertainties are calculated as described in Ref. [13].

3 Event selection

Muon candidates are reconstructed with the particle-flow (PF) algorithm [14], which reconstructs all particles produced in a collision simultaneously, based on information from all detector subsystems. Muon candidates are required to have $p_T > 30\,\text{GeV}$ and to be reconstructed within $|\eta| < 1.4442$, corresponding to the acceptance of the barrel of the ECAL. Only muons with at least ten measured hits in the silicon tracker and at least one hit in the pixel detector are considered. In addition, we require that the sum of energy from charged hadrons, neutral hadrons, and photons within a cone $\Delta R \equiv \sqrt{(\Delta\eta)^2 + (\Delta\phi)^2} = 0.3$ around the muon be less than p_T-dependent thresholds in order to ensure the candidate is isolated from other activity in the event.

Photons are reconstructed from energy deposits in the ECAL. We require the shape of ECAL clusters to be consistent with that expected for a photon, and we require that the energy present in the corresponding region of the HCAL does not exceed 5% of the ECAL energy. In order to ensure the photons are reconstructed with high efficiency, all photon objects are required to have $p_T > 40$ GeV and be within the barrel fiducial region of the detector ($|\eta| < 1.4442$). We require that the photon candidate be isolated and separated from any muons by $\Delta R > 0.3$. We further require that the photon candidate possess no pixel track seed, consisting of at least two hits in the pixel detectors consistent with a charged particle trajectory, to distinguish the candidate from an electron.

The selection of electron candidates is identical to that of photons, with the exception that the candidate is required to be matched to a pixel track seed consistent with a charged track, to ensure the selection is orthogonal to that of photons. Due to the equivalence of the ECAL response to electrons and photons, $Z\rightarrow$ ee events are used to measure the photon identification efficiency via the tag-and-probe method [15] in both data and simulation. The ratio of the efficiency in data and simulation was measured as a function of the p_T and η of the electron and the ΔR separation between the electron and the nearest jet. It is determined that this ratio does not depend significantly on any measured kinematic variables, and the overall ratio is computed to be $\epsilon_e^{\text{data}}/\epsilon_e^{\text{sim}} = 0.983 \pm 0.012$.

Jets are reconstructed via the anti-k_T clustering algorithm [16] from PF objects with a distance parameter of 0.4. The jet energy and momentum are corrected for both the nonlinear response of the detector and the effect of additional proton-proton collisions in the event (pileup) via the procedure described in Ref. [17]. Jets are required to have corrected $p_T > 30\,\text{GeV}$ and to be reconstructed within $|\eta| < 2.4$. In addition, jets are required to be separated from other objects in the event by $\Delta R > 0.4$.

For the purpose of defining the various control regions to be used in the analysis, we employ an additional set of selection criteria. Fake photons are defined as those photons passing the base selection but failing either the shape requirement for the ECAL clusters or the charged hadron isolation requirement.

Events are then sorted exclusively into one of four categories depending on the selection of their highest-p_T electromagnetic objects: $\gamma\gamma$, ee, fake-fake (ff), and eγ. For each of these categories, no requirement is made on the number of jets in the event. The signal selection region is defined by the events in the $\gamma\gamma$ category with $E_T^{\text{miss}} > 100\,\text{GeV}$ and split into four bins: $100 < E_T^{\text{miss}} < 110\,\text{GeV}$, $110 < E_T^{\text{miss}} < 120\,\text{GeV}$, $120 < E_T^{\text{miss}} < 140\,\text{GeV}$, and $E_T^{\text{miss}} > 140\,\text{GeV}$.

4 Estimation of backgrounds

The dominant background for this analysis comes from QCD processes without intrinsic $E_{\mathrm{T}}^{\mathrm{miss}}$, where the high-$E_{\mathrm{T}}^{\mathrm{miss}}$ signature is mimicked by the mismeasurement of the hadronic activity in the event, with a subdominant contribution from electroweak processes that include genuine $E_{\mathrm{T}}^{\mathrm{miss}}$ from neutrino production.

The contribution from the QCD background is modeled from the ee and ff control samples. These control samples differ in hadronic activity from the candidate $\gamma\gamma$ sample due to different event topologies. To account for this difference, the di-EM p_{T} variable is used to model the hadronic recoil in the event. The di-EM p_{T} is defined as the magnitude of the vector sum of the transverse momenta of the two electromagnetic objects. Events in the ee and ff control samples are reweighted by the di-EM p_{T} distribution of the $\gamma\gamma$ events to correct for any differences in hadronic recoil. The di-EM p_{T} distributions for the candidate sample and both control samples are shown in Figure 2, and the $E_{\mathrm{T}}^{\mathrm{miss}}$ distribution before and after reweighting is shown in Figure 3. The $E_{\mathrm{T}}^{\mathrm{miss}}$ distributions of these di-EM p_{T} reweighted control samples are then normalized to the $\gamma\gamma$ sample in the region $E_{\mathrm{T}}^{\mathrm{miss}} < 50\,\mathrm{GeV}$ and used to predict the contribution of QCD processes to the high-$E_{\mathrm{T}}^{\mathrm{miss}}$ signal region. A comparison of the reweighted $E_{\mathrm{T}}^{\mathrm{miss}}$ distributions to the distribution of $\gamma\gamma$ events is shown in Figure 4 in the sideband of the search region ($E_{\mathrm{T}}^{\mathrm{miss}} < 100\,\mathrm{GeV}$). There is very good agreement between the $\gamma\gamma$ and each of the reweighted distributions.

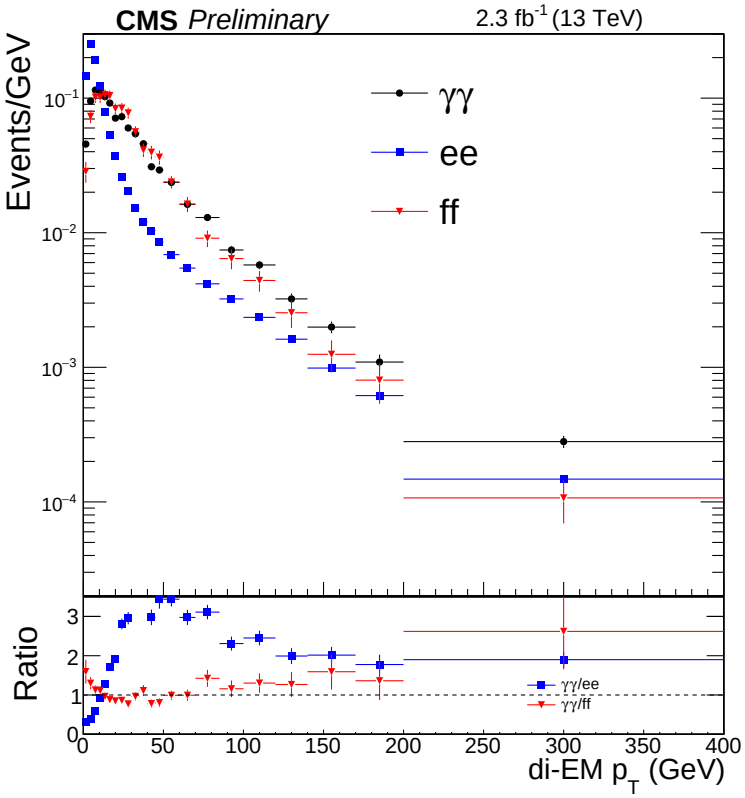

Figure 2: Di-EM p_{T} distribution of the $\gamma\gamma$ candidate sample and ee and ff control samples. The ratios of the candidate sample to each of the control samples are shown below. These ratios serve as the reweighting factors for the events.

Similarly, we consider differences in the $E_{\mathrm{T}}^{\mathrm{miss}}$ distribution due to the number of jets in the event. A direct comparison of the candidate sample and the two control samples shows little dependence on the jet multiplicity N_{jets}, so we take the small difference as a systematic uncertainty

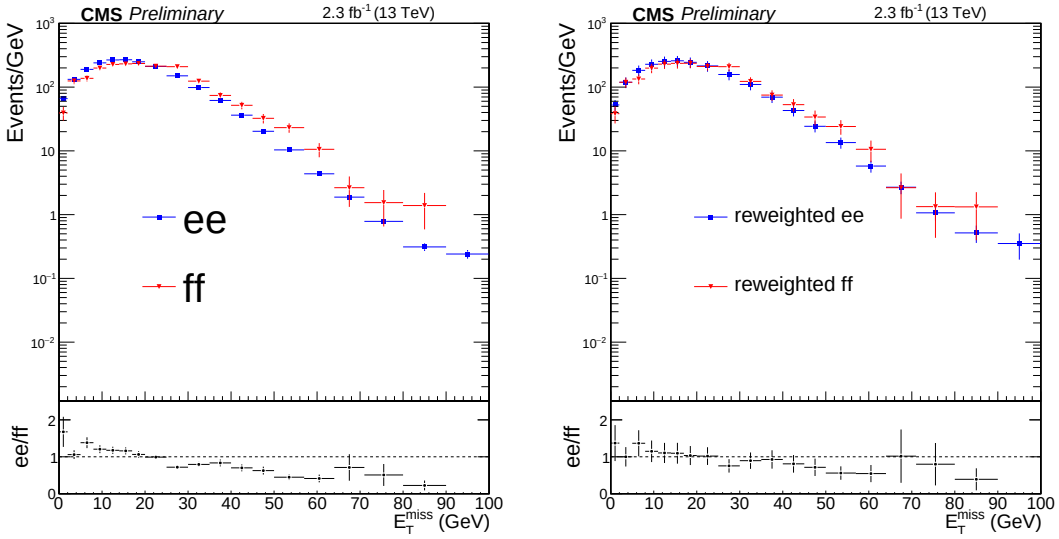

Figure 3: $E_{\mathrm{T}}^{\mathrm{miss}}$ distributions of the ee and ff control samples before (left) and after (right) reweighting by the di-EM p_{T} distribution.

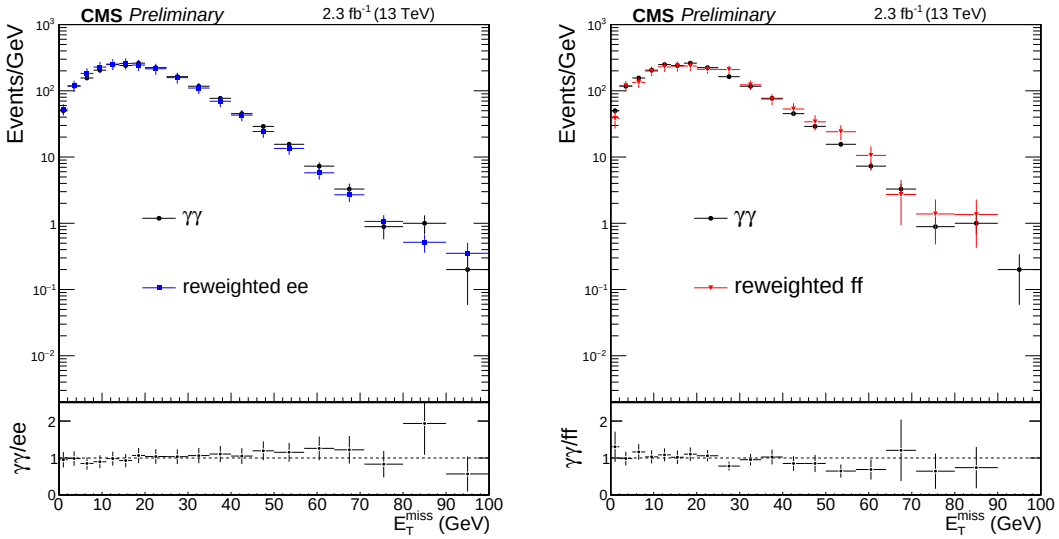

Figure 4: $E_{\mathrm{T}}^{\mathrm{miss}}$ distributions of the $\gamma\gamma$ and reweighted ee (left) and reweighted ff (right) control samples.

on the prediction.

In addition, there is a small contribution in the QCD control samples from comparatively rare processes with real E_T^{miss}, including $t\bar{t}$ events and $Z \to \nu_l\bar{\nu}_l$ + jets. Due to their small cross sections, these processes are estimated with simulation, and their contributions are subtracted from the ee and ff control samples for the final prediction.

The primary estimate of the QCD contribution comes from the ee distribution. The ff control sample serves as a cross check, and the difference from the prediction from the ff E_T^{miss} distribution and the ee E_T^{miss} distribution is taken as a systematic uncertainty on the prediction. Due to the limited number of ff events with $E_T^{miss} > 100\,\text{GeV}$, a looser fake definition is used to obtain the shape of the ff distribution in the $E_T^{miss} > 100\,\text{GeV}$ signal region, while the normalization comes from the tighter, more photon-like fake definition.

As an additional cross check on this background estimation method, we construct the ratio of the candidate $\gamma\gamma$ distribution to the unweighted ff distribution as a function of E_T^{miss} and fit this ratio to an exponential. The predicted number of events from the QCD background in each E_T^{miss} bin is then given by this function multiplied by the number of ff events seen in that bin. To give an uncertainty on this estimate, the fit parameters are varied by 1σ. The primary prediction from the ee sample is consistent with the prediction from this cross check within uncertainties, and we conclude that the predictions from these two methods are compatible.

The electroweak background comes from $W\gamma$ events where the W decays to an electron and a neutrino, and the electron is misidentified as a photon. We estimate this fake rate by comparing the peak from the Z boson in the ee invariant mass spectrum to the peak in the $e\gamma$ spectrum. The peak is modeled using an extended likelihood fit to the mass spectrum for the signal plus background hypothesis. The fake rate $f_{e\to\gamma}$ is then computed from the signal events as $f_{e\to\gamma} = N_{e\gamma}/(2N_{ee} + N_{e\gamma}) = (2.13 \pm 0.21)\%$. This rate is used to compute a scaling factor $f_{e\to\gamma}/(1 - f_{e\to\gamma})$, which is then applied to the sample of $e\gamma$ events with $E_T^{miss} > 100\,\text{GeV}$ to obtain our estimate of the electroweak background in the candidate selection region.

5 Sources of systematic uncertainty

We evaluate systematic uncertainties from each of the background predictions, the signal efficiency, and the luminosity. For each source of uncertainty, we describe the uncertainty value and the method used for its estimation.

The largest systematic uncertainties in the background prediction come from the QCD estimation method. We consider three sources of systematic uncertainty from the QCD estimation: from the di-EM p_{T} reweighting, from the jet multiplicity, and from the $E_{\mathrm{T}}^{\mathrm{miss}}$ shape difference between the ee and ff control samples.

The uncertainty from di-EM p_{T} reweighting is estimated from the generation of toy distributions of the di-EM p_{T} ratio, allowing the ratio to vary bin by bin according to a Gaussian distribution with a standard deviation computed from the statistical uncertainty of unweighted events in the bin. The $E_{\mathrm{T}}^{\mathrm{miss}}$ distribution of the ee control sample was then reweighted by each of these toy distributions, and the 1σ standard deviation was determined for the prediction. The magnitude of this uncertainty ranges from 15% to 39%.

The effect of the difference in the $E_{\mathrm{T}}^{\mathrm{miss}}$ distribution as a function of the jet multiplicity is determined directly by taking the difference between the ee estimate with di-EM p_{T} and N_{jets} reweighting and with di-EM p_{T} reweighting alone. The shape uncertainty of the ee control sample is determined by fitting the high-$E_{\mathrm{T}}^{\mathrm{miss}}$ tails of the ee and ff samples to the three parameter functional fit $\mathrm{d}N/\mathrm{d}E_{\mathrm{T}}^{\mathrm{miss}} = (E_{\mathrm{T}}^{\mathrm{miss}})^{p_0} e^{p_1 (E_{\mathrm{T}}^{\mathrm{miss}})^{p_2}}$. The systematic uncertainty in the shape is taken to be the fractional difference between the fitted functions for each $E_{\mathrm{T}}^{\mathrm{miss}}$ distribution. This yields a systematic effect between 12% and 150% depending on the signal $E_{\mathrm{T}}^{\mathrm{miss}}$ bin.

The main source of uncertainty in the electroweak background estimate comes from the uncertainty in the extended likelihood fit used to calculate the fake rate. This is computed by shifting the fake rate up and down by its uncertainty and scaling the $e\gamma$ $E_{\mathrm{T}}^{\mathrm{miss}}$ distribution by the altered fake rates. The difference between the estimates from the two shifted fake rates gives the systematic uncertainty in the rate of electroweak events. Because this represents an uncertainty in the overall normalization, it is constant across each $E_{\mathrm{T}}^{\mathrm{miss}}$ bin, found to be 19%.

The signal efficiency uncertainties are related to the statistical uncertainty from the finite size of the signal samples (0–16%), knowledge of the jet energy scale (0–23% depending on the $\widetilde{\mathrm{g}}$–$\widetilde{\chi}_1^0$ mass splitting), parton distribution function uncertainties (13–22% depending on signal point) and photon identification and reconstruction efficiencies (2.4%). The uncertainty related to the size of the data sample is 4.6%.

6 Results

The measured $E_{\mathrm{T}}^{\mathrm{miss}}$ distribution and corresponding background predictions are shown in Figure 5. In the signal region we observe 9 events, compared to an expected background of 7.2 ± 2.1. The data are seen to be in reasonable agreement with the background estimate within the uncertainties.

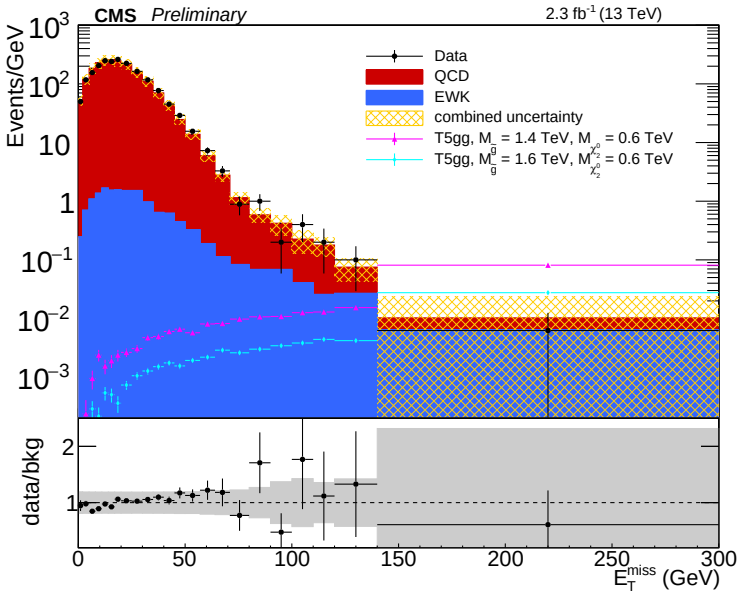

Figure 5: Measured $E_{\mathrm{T}}^{\mathrm{miss}}$ distribution in comparison with the background prediction in the signal region. The systematic uncertainty on the background prediction and the ratio of the data to the prediction are also shown.

We determine 95% confidence level (CL) upper limits on the gluino pair production cross section using the modified frequentist CLs method [18] based on a log-likelihood test statistic that compares the likelihood of the SM-only hypothesis to the likelihood of the presence of signal in addition to the SM contributions. The likelihood functions are based on the expected shape of the $E_{\mathrm{T}}^{\mathrm{miss}}$ distribution for signal and background in four separate bins, and the total likelihood is the product of each. The systematic uncertainties described in Section 5 are included in the test statistic as nuisance parameters, with log-normal probability distributions.

Figure 6 shows the expected reach of the analysis as a function of the gluino and neutralino masses. The predicted NLO + NLL cross section is used for each signal point, and the median expected mass exclusion includes a band representing the 1σ variation of the experimental uncertainties. For typical values of neutralino mass, we expect to exclude gluino masses out to 1.6 TeV, and we observe exclusions of 1.65 TeV, improving by approximately 300 GeV upon the reach of previous searches performed at center-of-mass energies of 8 TeV [19].

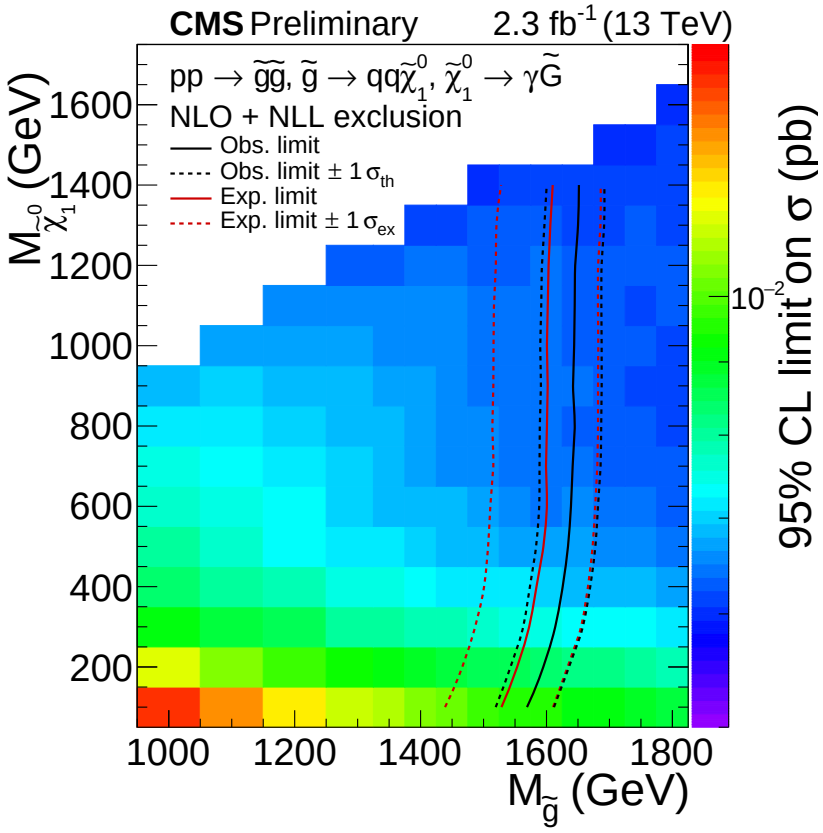

Figure 6: The 95% confidence level upper limits on the gluino pair production cross section as a function of gluino and neutralino masses. The countours show the observed and median expected exclusions assuming the NLO + NLL cross sections, with their one standard deviation uncertainties.

7 Summary

We perform a search for SUSY with general gauge mediation in events with two photons and large missing transverse energy using data from proton-proton collisions collected at center-of-mass energy $\sqrt{s} = 13\,\text{TeV}$ with the CMS detector in 2015, corresponding to an integrated luminosity of $2.32\,\text{fb}^{-1}$.

Using background estimation methods based on control samples in data, we determine limits on the gluino pair production cross section, and we use those limits together with NLO + NLL cross section calculations to constrain the masses of gluinos and neutralinos in the GGM framework. We exclude gluino masses below 1.65 TeV at a 95% CL, which represents an enhancement with respect to previous analyses performed in Run 1.

References

[1] P. Fayet, "Mixing Between Gravitational and Weak Interactions Through the Massive Gravitino", *Phys. Lett.* **B70** (1977) 461, doi:10.1016/0370-2693(77)90414-2.

[2] P. Fayet, "Scattering Cross-Sections of the Photino and the Goldstino (Gravitino) on Matter", *Phys. Lett.* **B86** (1979) 272, doi:10.1016/0370-2693(79)90836-0.

[3] P. Fayet, "Lower Limit on the Mass of a Light Gravitino from e^+ e^- Annihilation Experiments", *Phys. Lett.* **B175** (1986) 471, doi:10.1016/0370-2693(86)90626-X.

[4] P. Meade, N. Seiberg, and D. Shih, "General Gauge Mediation", *Prog. Theor. Phys. Suppl.* **177** (2009) 143–158, doi:10.1143/PTPS.177.143, arXiv:0801.3278.

[5] M. Buican, P. Meade, N. Seiberg, and D. Shih, "Exploring General Gauge Mediation", *JHEP* **0903** (2009) 016, doi:10.1088/1126-6708/2009/03/016, arXiv:0812.3668.

[6] S. Abel, M. J. Dolan, J. Jaeckel, and V. V. Khoze, "Phenomenology of Pure General Gauge Mediation", *JHEP* **0912** (2009) 001, doi:10.1088/1126-6708/2009/12/001, arXiv:0910.2674.

[7] CMS Collaboration, "The CMS experiment at the CERN LHC", *JINST* **3** (2008) S08004, doi:10.1088/1748-0221/3/08/S08004.

[8] J. Alwall et al., "The automated computation of tree-level and next-to-leading order differential cross sections, and their matching to parton shower simulations", *JHEP* **07** (2014) 079, doi:10.1007/JHEP07(2014)079, arXiv:1405.0301.

[9] T. Sjöstrand, S. Mrenna, and P. Skands, "PYTHIA 6.4 physics and manual", *JHEP* **05** (2006) 026, doi:10.1088/1126-6708/2006/05/026, arXiv:hep-ph/0603175.

[10] CMS Collaboration, "Interpretation of searches for supersymmetry with simplified models", *Phys. Rev. D* **88** (Sep, 2013) 052017, doi:10.1103/PhysRevD.88.052017.

[11] A. Kulesza and L. Motyka, "Soft gluon resummation for the production of gluino-gluino and squark-antisquark pairs at the LHC", *Phys. Rev.* **D80** (2009) 095004, doi:10.1103/PhysRevD.80.095004, arXiv:0905.4749.

[12] W. Beenakker et al., "Soft-gluon resummation for squark and gluino hadroproduction", *JHEP* **12** (2009) 041, doi:10.1088/1126-6708/2009/12/041, arXiv:0909.4418.

[13] M. Kramer et al., "Supersymmetry production cross sections in pp collisions at $\sqrt{s} = 7$ TeV", arXiv:1206.2892.

[14] CMS Collaboration, "Commissioning of the Particle-flow Event Reconstruction with the first LHC collisions recorded in the CMS detector", CMS Physics Analysis Summary CMS-PAS-PFT-10-001, 2010.

[15] CMS Collaboration, "Performance of Photon Reconstruction and Identification with the CMS Detector in Proton-Proton Collisions at sqrt(s) = 8 TeV", *JINST* **10** (2015), no. 08, P08010, doi:10.1088/1748-0221/10/08/P08010, arXiv:1502.02702.

[16] M. Cacciari, G. P. Salam, and G. Soyez, "The anti-k_t jet clustering algorithm", *JHEP* **04** (2008) 063, doi:10.1088/1126-6708/2008/04/063, arXiv:0802.1189.

[17] CMS Collaboration, "Determination of jet energy calibration and transverse momentum resolution in CMS", *JINST* **6** (2011) P11002, doi:10.1088/1748-0221/6/11/P11002.

[18] A. L. Read, "Modified frequentist analysis of search results (the CL_s method)", Technical Report CERN-OPEN-2000-205, 2000.

[19] CMS Collaboration, "Search for supersymmetry in two-photons+jet events with razor variables in pp collisions at sqrt(s) = 8 TeV", CMS Physics Analysis Summary CMS-PAS-SUS-14-008, 2014.